Dalton Transactions

Accepted Manuscript

ROYAL SOCIETY OF CHEMISTRY

www.rsc.org/dalton

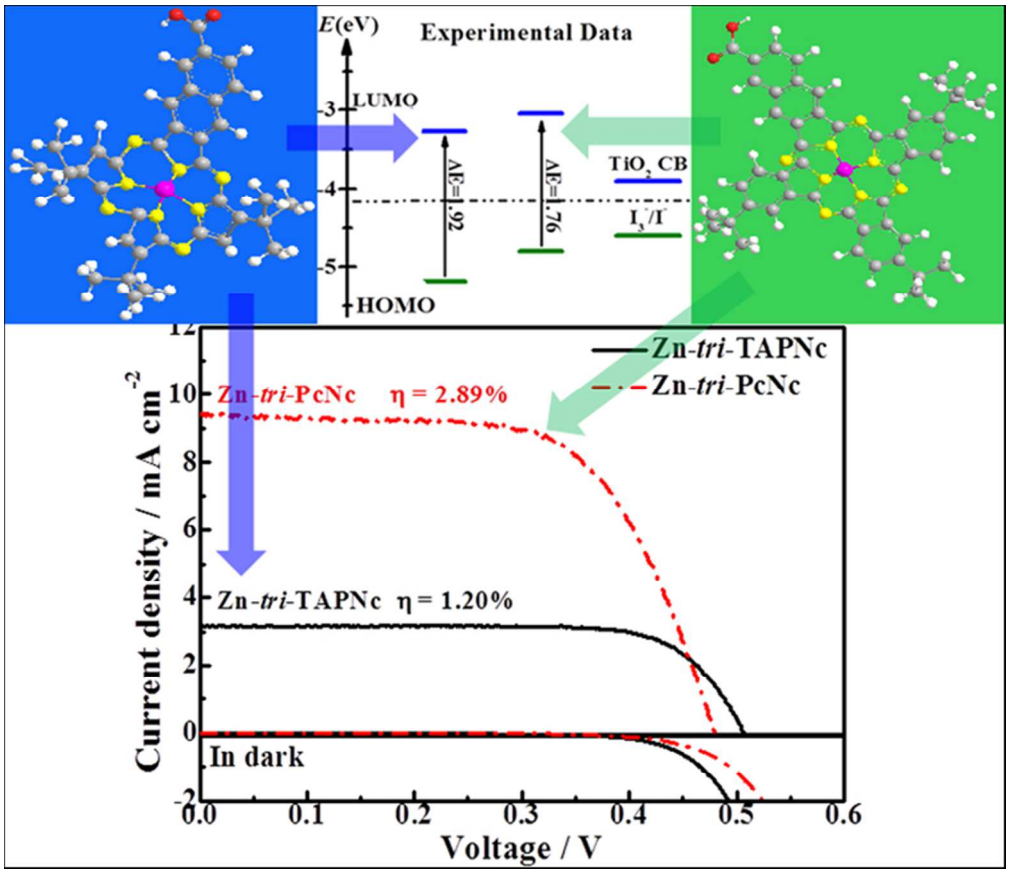

203x175mm (96 x 96 DPI)

Cite this: DOI: 10.1039/c0xx00000x

www.rsc.org/xxxxxx

ARTICLE TYPE

Effects of Benzo-Annelation of Asymmetric Phthalocyanine on the Photovolatic Performance of Dye-Sensitized Solar Cells

Lijuan Yu,[a] Wenye Shi,[a] Li Lin,[a] Yuwen Liu,[a] Renjie Li,*[,a] Tianyou Peng*[,a] and Xingguo Li[b]

Received (in XXX, XXX) Xth XXXXXXXXX 20XX, Accepted Xth XXXXXXXXX 20XX

DOI: 10.1039/b000000x

Novel highly asymmetric zinc tetraazaporphyrin (TAP) derivatives (Zn-*tri*-TAPNc and Zn-*tri*-PcNc) with one carboxyl and three *tert*-butyl peripheral substituent groups were synthesized. Highly asymmetric zinc phthalocyanine (ZnPc) derivative (Zn-*tri*-PcNc) has a benzo-annelated ring which contains tribenzonaphtho-condensed tetraazaporphyrin with the same peripheral substituents as Zn-*tri*-TAPNc. As sensitizer for TiO_2-based dye-sensitized solar cell, Zn-*tri*-PcNc derived from the benzo-annelation of TAP macrocycle showed improved light harvesting and electron injection efficiency, which can retard the charge recombination, and resulting in a great improvement in the incident photon-to-current conversion efficiency (IPCE). The Zn-*tri*-PcNc-sensitized solar cell exhibited a higher conversion efficiency (2.89%) than the Zn-*tri*-TAPNc-sensitized one (1.20%) under AM 1.5G solar irradiation. The present results on the TAP macrocycle's benzo-annelation demonstrate that optimization of molecular structure via changing the peripheral substituent group's "push-pull" effect and enlarging the conjugated π-system is an effective approach to improve the performance of tetraazaporphyrin-based dye-sensitized solar cell.

Introduction

Solar energy is one of several promising renewable energy sources that could contribute to a sustainable energy supply and mitigate the increasing energy shortages. Therefore, many researchers have engaged in developing cheap devices for the conversion of solar energy to electricity, and dye-sensitized solar cells (DSSCs) have been attracting increasing interests due to its relatively high performance and low-cost production as compared to the traditional silicon-based devices.[1-6] Generally, DSSCs are mainly composed of three major components: dye, redox electrolyte and photoanode. For many years, ruthenium-bipyridyl dye families such as N719, N3 and C101 are the most efficient dyes, and have dominated the highly efficient solar cells.[4-7] However, ruthenium is a rare metal and ruthenium-based dyes are usually lack of absorption in the red/near-IR light of the solar radiation. Therefore, it is imperative to extend the dye's spectral response range to the red/near-IR region so as to further improve the performance of the DSSCs. In the quest for ideal ruthenium-free dyes, porphyrins, phthalocyanines (Pcs) and their analogues with large conjugated π-system, which is suitable for the efficient electron transfer, are receiving considerable attention.[8-10]

Although tetraazaporphyrins (TAPs) are structural analogues of naturally occurring porphyrins, their spectral properties are very similar to Pcs because the replacement of the *meso*-carbons with nitrogen atoms causes a marked stabilization of the highest occupied molecular orbital (HOMO) energy level (HOMO-1).[11] In addition, the chemically and physically robust nature of TAPs is also analogous to Pcs.[12] As a kind of heterocyclic compound, TAP contains four pyrrole nuclei fused via nitrogen bridges and forms stable chelate with metal cation, which results in intense absorption in the UV/blue (Soret-band) and the red/near-IR (Q-band) region.[13-15] Moreover, the physical/chemical characteristics of the TAPs can be conveniently tuned through metal coordination or peripheral β-substituent.[16] The functional groups fused directly to the β-position of the pyrrole units can more strongly couple to the TAP macrocycle than those attached to the fused benzo-positions of Pcs.[14] Therefore, the functionalization by using different β-substituent groups can provide TAPs with novel electronic, optical and photophysical properties as well as greatly enhance the solubility in organic solvents as compared to their Pc counterparts.[17-19] As a result, their tunable electronic/optical properties render them especially suitable for acting as sensitizer in the dye-sensitized photovolatic devices.[18,19]

Herein, novel highly asymmetric zinc tetraazaporphyrin (ZnTAP) derivative (Zn-*tri*-TAPNc) with a carboxyl and three *tert*-butyl (*t*Bu) peripheral substituents was synthesized by using 6- carboxymethyl-2,3-dicyanonaphthalene and cis-1,2-dicyano-3,3-dimethyl-1-butylene as starting agents based on "push–pull" concept.[20] Zn-*tri*-TAPNc is a ZnTAP derivative containing three *t*Bu substitutes at the β-position of each pyrrole units and a carboxyl group at the naptho-part. The bulky *t*Bu groups as electron releasing (push) groups can enhance the solubility and minimize the molecule aggregation, while the carboxyl group can not only provide anchoring to the TiO_2, but also act as electron withdrawing (pull) group. Through the benzo-annelation of TAP macrocycle, Zn-*tri*-TAPNc was changed into ZnPc derivative (Zn-*tri*-PcNc) containing tribenzonaphtho-condensed TAP macrocycle with the same peripheral substituents. The detailed preparation procedures and spectroscopic characterization results

of Zn-*tri*-PcNc were given in our previous publication.[21] The molecular structures of TAP derivatives are listed in Scheme 1.

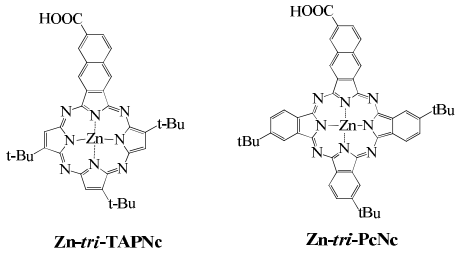

Scheme 1. Molecular structures of Zn-*tri*-TAPNc and Zn-*tri*-PcNc.

Zn-*tri*-TAPNc was synthesized according to the synthetic route shown in Scheme 2. Among those raw materials listed in Scheme 2, 6-carboxymethyl-2,3-dicyanonaphthalene (**4**) was prepared by the method reported elsewhere.[21] The benzo-annelation of Zn-*tri*-TAPNc was designed to extend the conjugated π-system, and then investigated its influence on the photoelectrochemical properties of the highly asymmetric TAP derivative in sensitization of TiO_2-based solar cell. It is found that the enlargement of the conjugated π-system from Zn-*tri*-TAPNc to Zn-*tri*-PcNc can cause an improvement of the molar extinction coefficient and a red-shift of the Q-band absorption, which leads to more effective near-IR light absorption and harvesting. Furthermore, the expanded conjugated π-system also causes a shift of the lowest unoccupied molecular orbital (LUMO) toward lower binding energy, which results in sufficient thermodynamic driving force for the electron injection from the excited dye to conduction band (CB) of TiO_2, and therefore Zn-*tri*-PcNc-sensitized solar cell shows better conversion efficiency than the Zn-*tri*-TAPNc-sensitized one. Moreover, electrochemical impedance spectra (EIS) and open-circuit voltage decay curves (OCVD) of those fabricated solar cells were used to explain the above results.

Experimental section

1. Chemicals

Dichlorobenzene for voltammetric studies was freshly distilled from CaH_2 under nitrogen. *n*-Butanol was distilled from sodium. Column chromatography was carried out on silica gel columns (Merck, Kieselgel 60, 70-230 mesh) with the indicated eluents. Preparative thin-layer chromatography (TLC) was performed on glass plates (20 cm × 20 cm) with silica gel GF-254. All solvents and reagents were of pure quality and used as received unless otherwise stated.

Asymmetric ZnPc derivative (Zn-*tri*-PcNc) containing tribenzo-naphtho-condensed porphyrazine with one carboxyl and three *tert*-butyl (*t*Bu) substituents was recently synthesized by us,[21] and some spectra of Zn-*tri*-PcNc were used in this work for comparison. The highly asymmetric zinc tetraazaporphyrin (ZnTAP) derivative (Zn-*tri*-TAPNc) was synthesized according to the synthetic route shown in Scheme 2. Among those raw materials listed in Scheme 2, 6-carboxymethyl-2,3-dicyano-naphthalene (**4**) was prepared by a method described elsewhere.[21]

2. Syntheses of dyes and precursor compounds

*2.1. Preparation of cis-1,2-dibromine-3,3-dimethyl-1-butylene (**2**)*

3,3-dimethyl-1-butyne (**1**) (500 mg, 6 mmol), benzoyl peroxide (BPO) (5 mg) and anhydrous n-hexane (10 mL) were added to the flask, and then cooled to -78°C. 1 mL bromine was added dropwise during 1 h under 125 W UV-lamp illumination. After stirring for 4 h, the solvent in the reaction mixture was evaporated under reduced pressure, and the resulting orange oily liquid was subjected to silica gel column chromatography with CH_2Cl_2 as eluent. The first band was cis-1,2-dibromine-3,3-dimethyl-1-butylene (**2**). Yield: 726 mg, 50%. ^{1}H NMR ($CDCl_3$, 300 MHz): δ=6.65 (s, 1H), 1.23 ppm (s, 9H).

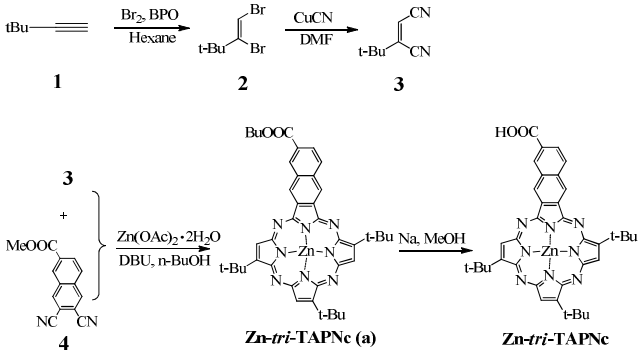

Scheme 2. Synthetic route to Zn-*tri*-TAPNc.

*2.2. Preparation of cis-1,2-dicyano-3,3-dimethyl-1-butylene (**3**)*

2 (100 mg, 0.4 mmol) was added to a solution of CuCN (74 mg, 0.82 mmol) in dry DMF (10 mL). After refluxing for 4 h, the resultant dark reaction mixture was poured into water and extracted with toluene, and the combined extracts were washed with water, dried with anhydrous $MgSO_4$, and then evaporated. The residue was purified by silica gel column chromatography with CH_2Cl_2 as eluent, giving white crystals after recrystallization in EtOH. Yield: 27 mg, 52%. ^{1}H NMR ($CDCl_3$, 300 MHz): δ=5.86 (s, 1H), 1.27 ppm (s, 9H).

2.3. Preparation of asymmetric Zn-tri-TAPNc

Zn-*tri*-TAPNc was prepared by a mixed cyclic tetramerization using 1:6 of **4** and **3** followed by ester hydrolysis with Na and methanol as shown in Scheme 2. Firstly, DBU (1 mL) was added into a suspension of 6-carboxymethyl-2,3- dicyanonaphthalene (**4**) (80 mg, 0.34 mmol), cis-1,2- dicyano-3,3-dimethyl -1-butylene (**3**) (270 mg, 2.0 mmol) and zinc acetate (222 mg, 1.0 mmol) in butanol (10 mL). After stirring for 12 h at 100°C under N_2, the solvent in the mixture was removed under reduced pressure. The solid material obtained was subjected to silica gel column chromatography with CH_2Cl_2 as eluent. The second band, a blue one, contained the desired asymmetric Zn-*tri*-TAPNc (a). Yield: 25 mg, 10%. ^{1}H NMR (DMSO-d_6, 300 MHz): δ=8.74 (s, 1H); 8.64 (s, 1H); 8.46 (s, 1H); 8.29-8.26 (d, 1H); 8.13-8.10 (d, 1H); 7.18 (s, 1H); 5.77 (s, 2H); 4.43-4.26 (m, 2H); 2.51 (s, 2H); 2.27-2.39 (m, 2H); 2.20 (s, 27H); 1.84-1.69 ppm (m, 3H); TOF-MS (*m*/*z*) calcd. for $C_{41}H_{44}N_8O_2Zn$ $[M+H]^+$ 746.23, found 745.55; Elemental Analysis calcd. for $C_{41}H_{44}N_8O_2Zn$: C 65.99; H 5.94; N 15.02. Found: C 66.23; H 5.68; N 15.52.

Secondly, 100 mg of compound Zn-tri-TAPNc (a) was dissolved in 25 mL methanol, and then added 1 g of Na. The resulting reaction mixture was stirred at room temperature for 7

days. The solvent was evaporated under reduced pressure. The obtained solid material was redissolved in water and pH value was adjusted to 3.00 by using dil. HCl. The precipitate was filtered and dried under reduced pressure to obtain the desired asymmetric Zn-*tri*-TAPNc. Yeild: 90 mg, 98%. ^{1}H NMR (DMSO-d_6, 300 MHz): δ=12.75 (s, 1H); 8.64-8.83 (m, 5H); 7.17 (s, 1H); 5.76 (s, 2H); 2.18 ppm (s, 27H); TOF-MS (*m*/*z*) calcd. for $C_{37}H_{36}N_8O_2Zn$ $[M+H]^+$ 690.12, found 690.41; Elemental Analysis calcd. for $C_{37}H_{36}N_8O_2Zn$: C 64.39; H 5.26; N 16.24. Found: C 63.85; H 5.30; N 15.89.

3. Fabrication of photoanode

The preparation of photoelectrode was performed by a doctor-blade technique on a conducting glass (FTO, 15-20 Ω sq^{-1}), which was rinsed with distilled water and fully soaked in isopropanol for 3 h to get rid of surface dirt and increase its hydrophilicity before use. The pre-treated FTO glass (Nippon Sheet Glass, 4 mm thickness) were firstly treated in $TiCl_4$ (50 mM) solution followed by calcination at 500^{o}C for 30 min. A paste composed of 20 nm anatase TiO_2 particles was spread on the treated FTO glass by adopting doctor-blade technique to obtain about 10 μm thickness, and then a paste for the scattering layer containing 200 nm anatase TiO_2 particles was twice deposited by adopting doctor-blade technique to obtain a thickness of about 4 μm after calcination at 500^{o}C for 30 min. The TiO_2 electrodes were then sintered at 500^{o}C for 30 min. In order to enhance the binding properties and connectivity of TiO_2 particles, the heated electrodes were impregnated with 25 mM $TiCl_4$ solution in water saturated desiccator for 30 min at 70^{o}C and washed with distilled water. The electrode area was protected from the $TiCl_4$ solution by adhesive tape. Finally, the TiO_2 electrode was sintered again at 500^{o}C for 30 min before dipping into dye solution.

4. Fabrication of DSSC

The TiO_2 electrode was immersed into the 5.0×10^{-5} M Zn-tri-TAPNc (or Zn-*tri*-PcNc) ethanol solutions for 12 h. 7.5 mM chenodeoxycholic acid (CDCA) was added into the above dye (Zn-*tri*-TAPNc or Zn-*tri*-PcNc) solution so as to reduce the dye molecule aggregation and improve the cell performance. The dye-sensitized electrode was assembled in a classic sandwich-type cell. Namely, the Pt counter electrode was attached on the dye-sensitized photoanode. After injection of the electrolyte solution (which consists of 0.5 M LiI, 0.05 M I_2, and 0.1 M 4-tert-butylpyridine in 15/85(v/v) mixture of valeronitrile and acetonitrile) into the interspace between the photoanode and the counter electrode, the photoelectrochemical property of DSSC was measured. In order to reduce scattered light from the edge of the glass electrodes of the dyed TiO_2 layer, a light-shading mask was used onto DSSC, fixing the active area of DSSC to 0.25 cm^2.

5. Dye measurement and characterization

^{1}H NMR spectra were recorded on a Bruker DPX 300 spectrometer (300 MHz) in $CDCl_3$ and DMSO-d_6. MALDI-TOF-MS spectra were taken on a Bruker BIFLEX III ultrahigh resolution Fourier transform ion cyclotron resonance (FT-ICR) mass spectrometer with alpha-cyano-4- hydroxycinnamic acid as matrix. Elemental analyses were performed on an Elementar Vavio El III. UV-vis absorption spectra were recorded on a Hitachi U-4100 spectrophotometer. Fluorescence spectra were recorded on K2 ISIS spectrometer. IR spectra were recorded as KBr pellets by using a BIORAD FTS-165 spectrometer with 2 cm^{-1} resolution.

Electrochemical measurements were carried out with a BAS CV-50W voltammetric analyzer. The cell comprised inlets for a glassy carbon disk working electrode of 3.0 mm in diameter and a silver-wire counter electrode. The reference electrode was Ag/Ag^+ (0.01 M), which was connected to the solution by a Luggin capillary whose tip was placed close to the working electrode. It was corrected for junction potentials by being referenced internally to ferrocenium/ferrocene (Fc^+/Fc) couple [$E_{1/2}$(Fc^+/Fc) = 0.50 V *vs*. SCE]. Typically, 0.1 M [Bu_4N][ClO_4] in dichlorobenzenc (DCB) containing 0.5 mmol dm^{-3} of sample was purged with nitrogen for 10 min, and then voltammogram was recorded at ambient temperature with scan rate of 20 mV s^{-1}.

6. Photoelectrochemical measurement of the solar cell

Electrochemical impedance spectroscopy (EIS) measurements were carried out by applying bias of the open-circuit voltage (V_{OC}) without electric current, and recorded over a frequency range of 10^{-2} to 10^5 Hz with ac amplitude of 10 mV. The solar cell was firstly illuminated to a steady voltage, and then the open-circuit voltage decay curve (OCVD) was recorded once the illumination was turned off by a shutter. Above measurements were carried out on a CHI-604C electrochemical analyzer (CH Instruments) combined with Xe-lamp.

The solar cell was illuminated by light with energy of 100 mW cm^{-2} from 300 W AM 1.5G simulated sunlight (Newport, 91160). The light intensity was determined using a SRC-1000-TC- QZ-N reference monocrystal silicon cell system (Oriel, USA), which was calibrated by National Renewable Energy Laboratory, A2LA accreditation certificate 2236.01. A computer-controlled Keithley 2400 source meter was employed to collect the photocurrent-voltage (*J*-*V*) curves. The incident photon-to-current conversion efficiency (IPCE) was measured as a function of wavelength from 250 to 900 nm by using a Model QE/IPCE system (PV Measurement Inc.).

7. Computational details

The primal input structures of Zn-*tri*-TAPNc (Scheme 1) were obtained by adding a naphthalene ring onto one of pyrrole rings of TAP and then attaching three *t*Bu groups and one carboxyl group onto the peripheral positions. The hybrid density functional Becke-Lee-Young-Parr composite of exchange-correlation functional method was used for both geometry optimizations and property calculations.[21] In all cases, the 6-31G (d) basis set was used. Berny algorithm using redundant internal coordinates was employed in energy minimization and the default cutoffs were used throughout. Using the energy-minimized structures generated in the previous step, normal coordinate analyses were carried out.

Results and discussion

1. Spectroscopic analyses

Fig. 1 shows the UV-vis absorption spectra of Zn-*tri*-TAPNc

and Zn-*tri*-PcNc dissolved in EtOH or adsorbed on TiO_2 film. As can be seen, both Zn-*tri*-TAPNc and Zn-*tri*-PcNc have maximum absorbence in the red/near-IR region. Zn-*tri*-TAPNc in EtOH solution shows a Soret-band absorption at 337 nm and two intense absorption bands at 612 and 643 nm in the Q-band region, and the molar extinction coefficient (ε) is 61840 mol^{-1} cm^{-1} at the maximum absorption wavelength (612 nm) as shown in Table 1. The above Q-band spliting is caused by the breakage of the symmetric π-system in Zn-*tri*-TAPNc, and the absorption bands at 612 and 643 nm can be attributed to $Q_{y0\text{-}0}$ and $Q_{x0\text{-}0}$ bands,[22] respectively. That is, an additional naphthalene group at one of the four pyrrole rings of the TAP macrocycle lowers the symmetry of the π-system and leads to the Q-band spliting into the intense Q_y ($S_0 \rightarrow S_{1y}$ transition) and Q_x ($S_0 \rightarrow S_{1x}$ transition).[22,23] Moreover, the Q-band (at 612 and 643 nm) of Zn-*tri*-TAPNc is dramatically blue-shifted as compared to that (694 nm) of Zn-*tri*-PcNc due to the absence of three benzo groups, which lowers the conjugated π-system and the electron delocalization extent of the whole ZnTAP molecule.[24] As shown in Table1, the molar extinction coefficient (ε) of Zn-*tri*-PcNc is 106000 mol^{-1} cm^{-1} at the maximum absorption wavelength (694 nm), which is 1.7 times as large as that of Zn-*tri*-TAPNc. Thus, it can be conjectured that Zn-*tri*-PcNc with extended π-system would absorb more photons, and then resulting in higher light harvesting efficiency than Zn-*tri*-TAPNc.

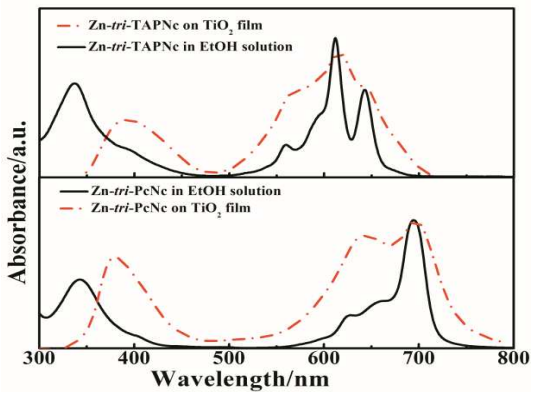

Fig. 1. UV-vis absorption spectra of Zn-*tri*-TAPNc and Zn-*tri*-PcNc dissolved in EtOH and adsorbed on TiO_2 film.

Zn-*tri*-TAPNc and Zn-*tri*-PcNc adsorbed on TiO_2 film show dramatically broadened Q-bands in the near-IR region as compared to the corresponding dyes in EtOH solution. This enlargement of Q-bands might be due to the adsorption and aggregation of the dye molecules on TiO_2 film.[25] Moreover, the Q-band absorption of Zn-*tri*-TAPNc on TiO_2 film also shows apparent blue-shift in comparison with Zn-*tri*-PcNc due to the absence of three fused benzo groups as mentioned above.[24] On the other hand, Zn-*tri*-TAPNc and Zn-*tri*-PcNc adsorbed on TiO_2 film shows an obvious red-shift in the Soret-band. The shift of Soret-band usually stems from the electronic transition from low energy level orbital to the LUMO orbital,[20] and therefore the above red-shift of Soret-band of Zn-*tri*-TAPNc and Zn-*tri*-PcNc can be attributed to the π-conjugated systems derived from part unoccupied molecule orbital of the adsorbed dye molecules coupling with TiO_2.[26]

Fluorescence spectra (Fig. 2) indicate that Zn-*tri*-TAPNc and Zn-*tri*-PcNc have the maximum emission peaks located at 661 and 711 nm, respectively. Accordingly, the optical bandgap ($E_{0\text{-}0}$) values can be estimated to be 1.92 eV for Zn-*tri*-TAPNc and 1.76 eV for Zn-*tri*-PcNc based on their corresponding absorption and emission spectra as shown in Fig. 2, Fig. S5 and Table 1.[27] The maximum emission band of Zn-*tri*-TAPNc shows a 50 nm blue-shift as compared to Zn-*tri*-PcNc, indicating Zn-*tri*-TAPNc has an optical bandgap widen by 0.16 eV as compared to Zn-*tri*-PcNc as shown in Table 1. Moreover, the newly prepared asymmetric Zn-*tri*-TAPNc has good solubility in common organic solvents such as ethanol, $CHCl_3$ and CH_2Cl_2, and the other satisfactory characterization results such as elemental analyses, MS and IR spectra are also obtained for Zn-*tri*-TAPNc as mentioned in the experimental section. For example, MALDI-TOF-MS spectra of the compounds clearly show intense signal of the molecular ion $(M)^+$, and the corresponding isotopic pattern closely resembles the simulated one as exemplified by the spectra of the TAP derivative and its precursor as given in Fig. S1 and S2 in the Supporting Information.

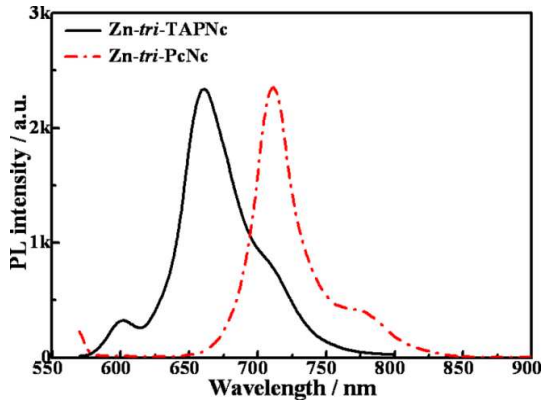

Fig. 2. Fluorescence emission spectra of Zn-*tri*-TAPNc and Zn-*tri*-PcNc in EtOH solution. Excitation fixed at 550 nm.

Moreover, the IR absorption bands (Fig. S3) of the ZnTAP derivatives are contributed by the aromatic TAP macrocycle core, which includes the wagging and torsion vibrations of C-H groups, stretching vibrations of iso-indole ring and C=N aza groups,[28] and the intensive IR absorption bands in the range of 3012-2800 cm^{-1} can be attributed to stretching vibrations of -COOH in ZnTAP derivatives. The characteristic IR bands of TAP dianion at ~1000 cm^{-1} can be attributed to the symmetric bending of C-H in $-CH_3$ groups of TAP ring together with the iso-indole stretching vibrations.[28]

2. Electrochemical analyses

To estimate the energy levels of the asymmetric ZnTAP derivatives and elucidate the effect of the extension of π-system on the energy levels, cyclic voltammetry (CV) was employed to investigate the electrochemical behavior of Zn-*tri*-TAPNc and Zn-*tri*-PcNc dissolved in 1,2-dichlorobenzene (DCB), and the corresponding results are listed in Fig. S4 and Table S1 (Supporting Information). As can be seen, Zn-*tri*-TAPNc displays two one-electron oxidation processes (labeled as Oxd_1 and Oxd_2) and up to three one-electron reduction processes (labeled as Red_1, Red_2 and Red_3) within the electrochemical window of DCB. The limited differences between the corresponding reduction and

oxidation peak potentials for both Zn-*tri*-TAPNc to Zn-*tri*-PcNc imply the reversible or quasi-reversible redox nature, which can be attributed to successive removal from or addition of one electron to the TAP ring-based orbitals.

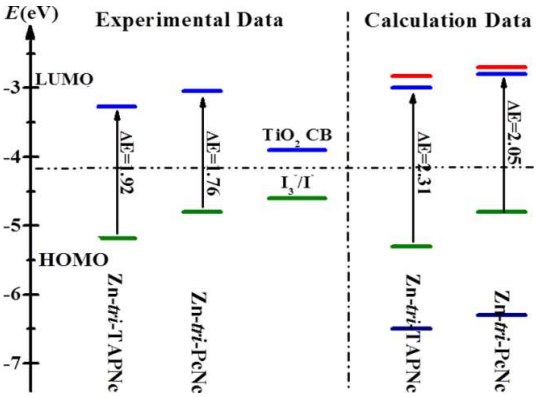

Fig. 3. Experimental measured (left) and theoretically calculated (right) molecular orbital energy levels of Zn-*tri*-TAPNc and Zn-*tri*-PcNc.

Dye energy levels (for instance, the LUMO level corresponds to the excited-state oxidation potential, while HOMO to the first oxidation potential) are crucial to electron injection and dye regeneration during the DSSC operations.[29] As can be seen from Table 1, Zn-*tri*-TAPNc and Zn-*tri*-PcNc have the first oxidation potentials (E_{ox}) of 0.75 V and 0.36 V, respectively. According to Leeuw's exprerence fomula shown in Table 1,[30] the HOMO levels of Zn-*tri*-TAPNc and Zn-*tri*-PcNc can be estimated to be -5.46 eV and -5.07 eV, respectively. It indicates that the HOMO energy levels for Zn-*tri*-TAPNc and Zn-*tri*-PcNc are more negative than I_3^-/I^- redox potential (-4.9 eV) as shown in Fig. 3.[31] Therefore, there is theoretically enough driving force for the regeneration of the excited dyes through recapturing electrons from I^- in the electrolyte.[31] Moreover, the lower HOMO level (-5.46 eV) of Zn-*tri*-TAPNc than that (-5.07 eV) of Zn-*tri*-PcNc can be ascriable to its more the extended π-system as compared to Zn-*tri*-TAPNc, which causes a shift of the HOMO level for Zn-*tri*-PcNc toward higher binding energy,[32] and then resulting in more negative HOMO level of Zn-*tri*-TAPNc. Namely, the energy level differences between the I^-/I_3^- redox potential and the HOMO level of Zn-*tri*-TAPNc is larger than that between the I^-/I_3^- redox potential and the HOMO level of Zn-*tri*-PcNc. It means that Zn-*tri*-TAPNc would larger dye regeneration ability than Zn-*tri*-PcNc.

On the other hand, the LUMO level of Zn-*tri*-TAPNc and Zn-*tri*-PcNc can be evaluated from the equation: $E_{LUMO} = (E_{HOMO} + E_{0-0})$ eV,[30] in which E_{0-0} is the 0-0 excitation and can be estimated from the absorption and emission spectra as shown Fig. 2 and Fig S5. The LUMO levels of Zn-*tri*-TAPNc and Zn-*tri*-PcNc can be estimated to be -3.54 and -3.31 eV, respectively. It indicates that the LUMO energy levels of both Zn-*tri*-TAPNc and Zn-*tri*-PcNc are higher than TiO_2 CB edge (-3.9 eV).[30,31] Therefore, there is sufficient driving force for the electron injection from the excited dye to TiO_2. Moreover, the LUMO level (-3.31 eV) of Zn-*tri*-PcNc is higher than that (-3.54 eV) of Zn-*tri*-TAPNc as shown in Fig. 3, which would provide more sufficient thermodynamic driving force for electron injection from the excited dye to TiO_2, and then resulting in more efficient electron injection efficiency of Zn-*tri*-PcNc.

To gain an insight into the molecular orbital energy levels of ZnTAP derivatives, density functional theory (DFT) calculation was carried out on Zn-*tri*-TAPNc and Zn-*tri*-PcNc within the framework of the DFT method at the B3LYP/6-31G(d) level. As shown in Fig. S6, the HOMO level of Zn-*tri*-TAPNc is delocalized over the whole molecule, and the LUMO is a π* orbital delocalized across the TAP ring moving to the carboxyl group, and the LUMO+2 is a π* orbital that is mainly localized over the TAP ring and further move to the carboxyl group. This indicates that the photoexcited electrons can transfer from the TAP skeleton to the carboxyl group, which is a benefit to the injection of the photoexcited electrons to the TiO_2.

Table 1 UV-vis absorption and electrochemical data of Zn-*tri*-TAPNc and Zn-*tri*-PcNc.

Dye	λ_{max} / nm	ε / mol^{-1} cm^{-1}	$E_{1/2}$ / V *vs.* SCE Ox	Red	E_{0-0} / eV	HOMO[a] / eV	LUMO[b] / eV
Zn-*tri*-TAPNc	612	61840	0.75	-1.03	1.92	-5.46	-3.54
Zn-*tri*-PcNc	694	106000	0.36	-1.13	1.76	-5.07	-3.31

[a] Calculated with the formula EHOMO = -(Eox+4.71) eV.
[b] Calculated with the formula $E_{LUMO} = (E_{HOMO} + E_{0-0})$ eV.

Similar distribution can also be observed for Zn-*tri*-PcNc, indicating that the molecule may also provide efficient electron injection into TiO_2. As shown in Fig. 3, the molecular orbital energy levels rise along the variation of molecular structures from Zn-*tri*-TAPNc to Zn-*tri*-PcNc. Both HOMO levels of Zn-*tri*-TAPNc and Zn-*tri*-PcNc are essentially isolated from the HOMO-1, which lie at 1.18 eV and 1.47 eV below their respective HOMO levels. Although LUMO+1 level of Zn-*tri*-TAPNc lies at 0.17 eV above its LUMO orbital, the LUMO+1 level of Zn-*tri*-PcNc only locates at 0.05 eV above its LUMO level. This may be ascribed to the different peripheral functional groups connected to the TAP marcpcycle, and the *t*Bu groups fused directly to the β-positions of the pyrrole units can more strongly couple to the TAP macrocycle than those attached to the fused benzo-positions of Pcs.[14] Moreover, the conjugated π-electron system of the naphthalene fused to the pyrrole ring is relatively independent from TAP marcocycle for the Zn-*tri*-TAPNc, which leads to the destabilization of the HOMO orbital of Zn-*tri*-TAPNc, and therefore addition of a naphthalene group to the TAP marcocycle results in an more obvious energy splitting between LUMO and LUMO+1 for Zn-*tri*-TAPNc.[32]

As for the Zn-*tri*-PcNc, the three fused benzo groups containing electron donating *t*Bu groups can efficiently couple with the conjugated π-electron system of the naphthalene fused to the pyrrole rings, which leads to higher the conjugation degree of Zn-*tri*-PcNc as compared to Zn-*tri*-TAPNc, and therefore, Zn-*tri*-PcNc only shows very small difference between the LUMO+1 and LUMO levels. Moreover, the theoretically calculated HOMO and LUMO levels of both dyes are very similar to the corresponding experimental values derived from the above spectroscopic and electrochemical analysis results, which can validiate the above conclusions on the electron injection and regeneration of the two dyes during the DSSC operations.

3. Solar cells' photovoltaic performance analyses

For evaluating the photovoltaic performances of the asymmetric Zn-*tri*-TAPNc and Zn-*tri*-PcNc as sensitizers for the

TiO_2-based solar cells, the current-voltage (*J-V*) curves of the solar cells fabricated with Zn-*tri*-TAPNc- or Zn-*tri*-PcNc-sensitized TiO_2 electrodes under simulated AM 1.5G one sun illumination (100 mW cm^{-2}) were measured and shown in Fig. 4, its corresponding short-circuit currents (J_{sc}), open-circuit potentials (V_{oc}), fill factors (FF) and overall conversion efficiencies (η) are summarized in Table 2. As can be seen, Zn-*tri*-PcNc-sensitized solar cell shows a much higher J_{sc} value and overall conversion efficiency (2.89%) than the Zn-*tri*-TAPNc-sensitized one (1.20%).

The differences in J_{sc} and efficiency between the two solar cells can be ascribed to their different light harvesting efficiencies in the Q-band region since the molar extinction coefficient of Zn-*tri*-PcNc is 1.7 times as that of Zn-*tri*-TAPNc as mentioned above. The increscent molar extinction coefficient is mainly caused by the addition of the three fused benzo groups to Zn-*tri*-TAPNc, which results in enhanced π-electron conjugation and delocalization extent over the whole molecule as mentioned above. Moreover, Zn-*tri*-PcNc has higher LUMO level than Zn-*tri*-TAPNc, which results in larger driving force for electron injection from the excited dye to TiO_2 as shown in Fig. 3. The higher electron injection efficiency of Zn-*tri*-PcNc caused by its larger driving force can also contribute to its J_{sc} value. The dark current value for the Zn-*tri*-PcNc-sensitized solar cell is smaller than that of the Zn-*tri*-TAPNc-sensitized one, also indicating that the injected electron recombination with I_3^- in the electrolyte is significantly retarded, which can also contribute the higher J_{sc} value of the Zn-*tri*-PcNc-sensitized solar cell.

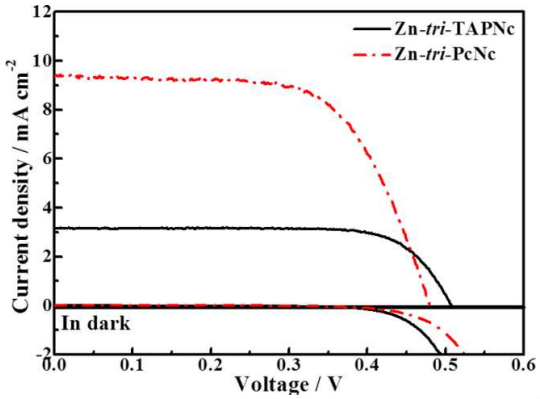

Fig. 4. Current-voltage and dark current characteristics of DSSCs sensitized by Zn-*tri*-TAPNc and Zn-*tri*-PcNc.

However, the V_{oc} value of Zn-*tri*-TAPNc-sensitized solar cell is increased by 30 mV as compared to Zn-*tri*-PcNc-sensitized one. On the one hand, the higher V_{oc} value of Zn-*tri*-TAPNc-sensitized solar cell can be attributed to its larger FF value than Zn-*tri*-PcNc-sensitized one as shown in Table 2. As mentioned above, the energy level differences between the I^-/I_3^- redox potential and the HOMO level of Zn-*tri*-TAPNc is larger than that of Zn-*tri*-PcNc, which results in the higher FF value, and then a higher V_{oc} value of the Zn-*tri*-TAPNc-sensitized solar cell than the Zn-*tri*-PcNc sensitized one.[33] On the other hand, the addition of the three fused benzo groups to Zn-*tri*-TAPNc results in enhanced π-electron conjugation and delocalization extents over the whole molecule, which leads to more efficient electronic coupling between the LUMO level of Zn-*tri*-PcNc and Ti 3d orbital.[20] This good coupling between Zn-*tri*-PcNc and TiO_2 seems to provide possibility for lowering the Femi energy levels of TiO_2, and then leads to a lower V_{oc} of Zn-*tri*-PcNc-sensitized solar cell than Zn-*tri*-TAPNc sensitized one.

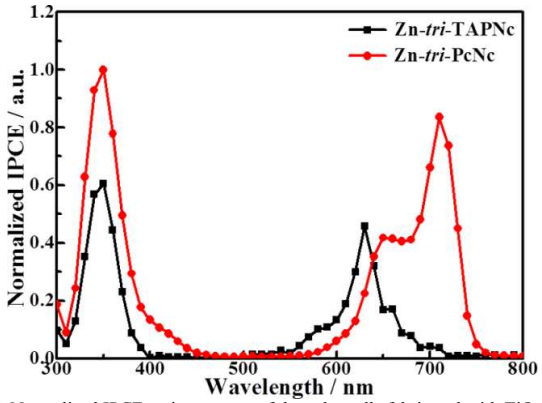

Fig. 5. Normalized IPCE action spectra of the solar cells fabricated with TiO_2 film electrodes sensitized by Zn-*tri*-TAPNc and Zn-*tri*-PcNc.

Fig. 5 shows the photocurrent action spectra of the solar cells fabricated with Zn-*tri*-TAPNc or Zn-*tri*-PcNc-sensitized TiO_2 electrode. As can be seen, the incident monochromatic photon-to-current conversion efficiency (IPCE) of TiO_2 film sensitized by Zn-*tri*-TAPNc is much lower than that of Zn-*tri*-PcNc, especially in the Q-band region, implying the poorer electron injection efficiency or more serious charge recombination in the Zn-*tri*-TAPNc-sensitized solar cell. The Q-band region of Zn-*tri*-TAPNc shows a dramatic blue-shift compared to Zn-*tri*-PcNc, which correlates well with the UV-vis absorption spectra. In addition, Zn-*tri*-TAPNc has a much lower spectral response in the Q-band range, which can also be explained by the low molar extinction coefficient mentioned above except for the poor electron injection efficiency or serious charge recombination. As can be seen, the lower performance of Zn-*tri*-TAPNc than Zn-tri-PcNc can be attributed to the lower light harvesting efficiency and the poor electron injection efficiency.

4. Solar cells' photoelectrochemical behavior analyses

The electrochemical impedance spectra (EIS) of those fabricated solar cells were measured and shown in Fig. 6. Generally, Nyquist plot features three semicircles that in the order of increasing frequency are attributed to the Nernst diffusion within the electrolyte, the electron transfer at the oxide/electrolyte interface, and the redox reaction at the Pt counter electrode. As can be seen from Fig. 6a, two semicircles can be observed, and the semicircle attributed to the Nernst diffusion within the electrolyte is featureless due to the relatively fast diffusion of the electrolyte in the porous films.[34] Therefore, a simple equivalent circuit model (inset of Fig. 6a) was used to simulate the present DSSCs.[34] Among those, R_s represents the serial resistance, which is mainly influenced by the sheet resistance of the substrate and electrical contact between the conductive glass/TiO_2 interfaces, R_{ct1} represents the impedance with charge transfer at the Pt counter electrode and/or electrical contact between TiO_2 nanoparticles, and R_{ct2} represents the impedance related to charge transfer process at TiO_2/dye/electrolyte interfaces.[35] R_{ct2} will be discussed in details because it relates significantly to the used dyes. The electron lifetime (τ_n) can be drawn by the positions of the low frequency peak in the Bode phase plots of EIS spectra

shown in Fig. 6b through $\tau_n = 1/2\pi f$ (f means the frequency of superimposed ac voltage). Furthermore, the effective rate constant (k_{eff}) for the recombination reaction can be also obtained according to the method proposed by Adachi.[36] The fitted R_{ct2}, τ_n, and k_{eff} values for those DSSCs are shown in Table 2.

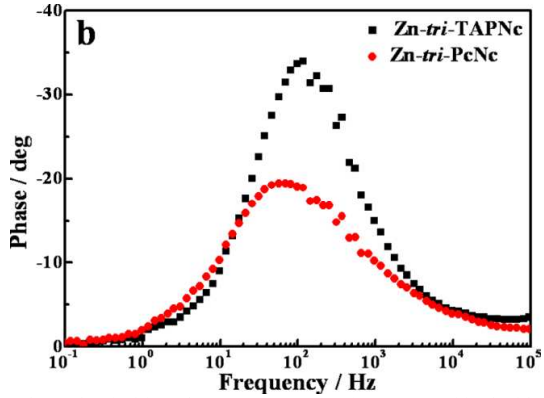

Fig. 6. Electrochemical impedance spectra (EIS) of DSSCs sensitized with Zn-*tri*-TAPNc and Zn-*tri*-PcNc. (a) Nyquist plots; (b) Bode phase plots.

As shown in the Nyquist plots (Fig. 6a), the smaller and larger semicircles are attributed to the charge-transfer at Pt counter electrode and the electron transport at TiO_2/dye/electrolyte interfaces, respectively. As can be seen from Table 2, the R_{ct2} value (42.9 Ω) of Zn-*tri*-PcNc-sensitized solar cell is greatly reduced as compared to that (90.0 Ω) of the Zn-*tri*-TAPNc-sensitized one. Because R_{ct2} represents the impedance related to charge transfer process at TiO_2/dye/electrolyte interfaces, it can be inferred that the charge combination rate between the injected electron and the electron acceptor (I_3^-) in the electrolyte are lowered as the π-system extends from Zn-*tri*-TAPNc to Zn-*tri*-PcNc. As stated above, introducing three fused benzo groups to Zn-*tri*-TAPNc significantly improves the molar extinction coefficient and expands the spectral response range of the solar cell to longer wavelength. Consequently, the near-IR light can be effectively absorbed, and then resulting in much enhanced light harvesting efficiency. Due to the increased light harvesting efficiency, more electrons can be excited from HOMO to LUMO of Zn-*tri*-PcNc, the injected rate of electrons in the dye LUMO levels to CBs of TiO_2 can be accelerated, and therefore the TiO_2/dye interface resistance decreased significantly. According to the f values of those Bode phase plots in Fig. 6b, the electron lifetimes (τ_n) can be calculated to be 2.77 and 1.36 ms for the Zn-*tri*-TAPNc- and Zn-*tri*-PcNc-sensitized solar cells, respectively. Moreover, the corresponding effective rate constant (k_{eff}) for the recombination reactions are 361 and 736 s^{-1}. Obviously, the benzo-annelation of Zn-*tri*-TAPNc is beneficial for promoting the electron lifetime and decreasing the effective rate constant of the recombination reaction. It implies that the back reaction of the injected electron with I_3^- in electrolyte can be efficient suppressed, which is consistent with the above photoelectrochemical analyses and the dark current shown in Fig. 4.

Open-circuit voltage decay (OCVD) curves can show the main information of the recombination process between the injected electrons in TiO_2 and the electrolyte under the dark state.[37] The lifetime (τ_n', response time of recombination reaction) of the injected electrons in TiO_2 is given by the reciprocal of the derivative of the decay curve normalized by the thermal voltage as follows.

$$\tau_n' = -\frac{k_B T}{e}\left(\frac{dV_{oc}}{dt}\right)^{-1} \quad (1)$$

where k_B is the Boltzmann coefficient, T is the temperature, and e is the elementary charge.

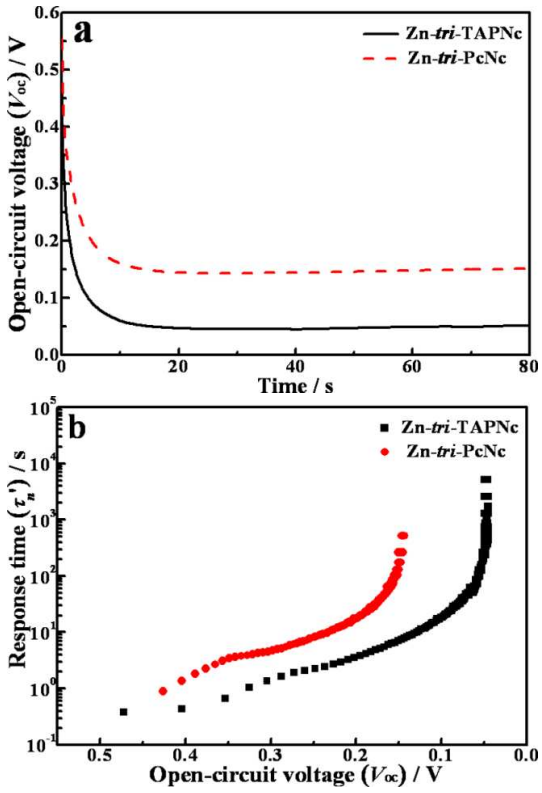

Fig. 7. OVCD curves (a) and corresponding τ_n'~V_{oc} curves (b) of the DSSCs sensitized with Zn-*tri*-TAPNc and Zn-*tri*-PcNc.

Table 2 Photoelectrochemical parameters of DSSCs sensitized by Zn-*tri*-TAPNc and Zn-*tri*-PcNc.

Dye	V_{oc} /V	J_{sc} /mA cm^{-2}	η / %	FF	R_{ct2} /Ω	f /Hz	τ_n /ms	k_{eff} /s^{-1}
Zn-*tri*-TAPNc	0.51	3.16	1.20	0.74	90.0	117.2	1.36	736
Zn-*tri*-PcNc	0.48	9.42	2.89	0.64	42.9	57.4	2.77	361

As shown in Fig. 7a, the decay trend of the V_{oc} values for the Zn-*tri*-TAPNc-sensitized solar cell is much faster than that of the Zn-*tri*-PcNc-sensitized one, indicating an extension of the π-system from Zn-*tri*-TAPNc to Zn-*tri*-PcNc can retard the charge recombination. It is also consistent with the above conclusion. Fig. 7b shows the influence of the benzo-annelation of Zn-*tri*-TAPNc on the τ_n' value of the solar cells. According to Bisquert's viewpoint,[36] the τ_n'-V_{oc} curves can be marked off as three voltage-dependent regions: 1) a constant lifetime at high V_{oc} region mainly dominated by the electron transfer process from the conduction band of TiO_2 to the electrolyte; 2) an exponential increase region due to the internal trapping and/or detrapping; and 3) an inverted parabola at low V_{oc} region coming from the effect of surface states.

As can be seen from Fig. 7b, the shapes of the τ_n'-V_{oc} curves for the Zn-*tri*-PcNc or Zn-*tri*-TAPNc-sensitized solar cell at the low V_{oc} regions are inverted parabola, indicating that the dye

molecules play an important role on the TiO_2 electrode surface. The τ_n' value is close to constant at the high V_{oc} region for Zn-*tri*-TAPNc-sensitized solar cell, indicating that the electron transfer from the TiO_2 CBs to the electrolyte is faster than Zn-*tri*-PcNc-sensitized one. Moreover, the overall τ_n'-V_{oc} curve for the Zn-*tri*-PcNc-sensitized solar cell moves upward as compared to the Zn-*tri*-TAPNc-sensitized one, implying longer lifetime of the injected electrons in the solar cell, and this longer lifetime of the injected electrons causes the improvement of the electron injection efficiency and in turn improves the photovoltaic characteristics.

Conclusions

In summary, this investigation reported the design, synthesis and characterization of novel highly asymmetric zinc tetraazaporphyrin (ZnTAP) derivative (Zn-*tri*-TAPNc). A significant effect of benzo-annelation of the ZnTAP on the performances of the dye-sensitized solar cell has been witnessed. It is found that the enlargement of the conjugated π-system from Zn-*tri*-TAPNc to Zn-*tri*-PcNc causes an obviously enhanced molar extinction coefficient and a red-shift of the Q-band, which lead to more effective near-IR light absorption and light harvesting. Moreover, the extended π-system causes a shift of the LUMO toward higher binding energies, and then results in sufficient thermodynamic driving force for the electron injection from the excited dye to TiO_2. Thus, Zn-*tri*-PcNc-sensitized solar cell shows better performance than the Zn-*tri*-TAPNc- sensitized one. Advantageously, Zn-*tri*-PcNc-sensitized solar cell shows longer electron lifetime and smaller effective rate constant of the recombination reaction than the Zn-*tri*-TAPNc- sensitized one. The present results on the benzo-annelation of Zn-*tri*-TAPNc indicates that phthalocyanine derivatives may be more suitable sensitizer for DSSCs in comparison with tetraazaporphyrin, and can also shed light on the efficient light harvesting and improvement of the photovoltaic performance of the phthalocyanine or porphyrin dye-sensitized solar cells via changing the peripheral substituents' "push-pull" effect and extending the conjugated π-system.

Acknowledgements

This work was supported by the Natural Science Foundation of China (21271146, 21271144, and 20973128), the Program for New Century Excellent Talents in University of China (NCET-07-0637), and the Beijing National Laboratory for Molecular Sciences (BNLMS).

Notes and references

[a] *College of Chemistry and Molecular Science, Wuhan University, Wuhan 430072, P. R. China. Fax: +86-27 6875 2237; Tel: +86-27 6875 2237;*
E-mail: typeng@whu.edu.cn (T. Peng)
E-mail: lirj@whu.edu.cn (R. Li)
[b] *Beijing National Laboratory for Molecular Sciences (BNLMS), College of Chemistry and Molecular Engineering, Peking University, Beijing 100190, China*

† Electronic Supplementary Information (ESI) available: [details of any supplementary information available should be included here]. See DOI: 10.1039/b000000x/

1 a) B. O'Regan and M. Grätzel, *Nature*, 1991, **353**, 737; b) S. Ito, M. K. Nazeeruddin, P. Liska, P. Comte, R. Charvet, P. Pechy, M. Jirousek, A. Kay, S. M. Zakeeruddin and M. Grätzel, *Prog. Photovolt: Res. Appl.*, 2006, **14**, 589.
2 a) K. Fan, T. Y. Peng, J. N. Chen, X. H. Zhang and R. J. Li, *J. Mater. Chem.*, 2012, **22**, 16121; b) J. N. Chen, T. Y. Peng, K. Fan, R. J. Li and J. B. Xia, *Electrochimica. Acta*, 2013, **94**, 1; c) K. Fan, T. Y. Peng, J. N. Chen, X. H. Zhang and R. J. Li, *J. Power Sources*, 2013, **222**, 38.
3 L. Alibabaei, J. M. Kim, M. Wang, N. Pootrakulchote, J. Teuscher, D. Di Censo, R. Humphry-Baker, J. E. Moser, Y. J. Yu, K. Y. Kay, S. M. Zakeeruddin and M. Gratzel, *Energy Environ. Sci.*, 2010, **3**,1757.
4 C. Y. Chen, S. J. Wu, C. G. Wu, J. G. Chen and K. C. Ho, *Angew. Chem. Int. Ed.*, 2006, **45**, 5822.
5 B. S. Chen, K. Chen, Y. H. Hong, W. H. Liu, T. H. Li, C. H. Lai, P. T. Chou, Y. Chi and G. H. Lee, *Chem. Commun.*, 2009, 5844.
6 Y. Cao, Y. Bai, Q. Yu, Y. Cheng, S. Liu, D. Shi, F. Gao and P. Wang, *J. Phys. Chem. C*, 2009, **113**, 6290.
7 a) M. Grätzel, *Acc. Chem. Res.*, 2009, **42**, 1788; b) M. K. Nazeeruddin, F. De Angelis, S. Fantacci, A. Selloni, G. Viscardi, P. Liska, S. Ito, T. Bessho and M. Grätzel, *J. Am. Chem. Soc.*, 2005, **127**, 16835.
8 I. Radivojevic, G. Bazzan, B. P. Burton-Pye, K. Ithisuphalap and R. Saleh, *J. Phys. Chem. C*, 2012, **116**, 15867.
9 M. T. Brumbach, A. K. Boal and D. R. Wheeler, *Langmuir*, 2009, **25**, 10685.
10 A. Yella, H. W. Lee, H. N. Tsao, C. Yi, A. K. Chandiran, M. K. Nazeeruddin, E. W. Diau, C. Y. Yeh, S. M. Zakeeruddin and M. Grätzel, *Science*, 2011, **334**, 629.
11 a) N. D. Hammer, S. Lee, B. J. Vesper, K. M. Elseth, B. M. Hoffman, A. G. M. Barrett and J. A. Radosevich, *J. Med. Chem.*, 2005, **48**, 8125; b) T. Fukuda and N. Kobayashi, *Dalton. Trans.*, 2008, 4685.
12 M. J. Fuchter, B. J. Vesper, K. A. Murphy, H. A. Collins, D. Phillips, A. G. M. Barrett and B. M. Hoffman, *J. Org. Chem.*, 2005, **70**, 2793.
13 M. P. Donzello, D. Dini, G. D'Arcangelo, C. Ercolani, R. Zhan, Z. Ou, P. A. Stuzhin and K. M. Kadish, *J. Am. Chem. Soc.*, 2003, **125**, 14190.
14 N. Kobayashi, *Coord. Chem. Rev.*, 2002, **227**, 129.
15 T. Imamura and K. Fukushima, *Coord. Chem. Rev.*, 2000, **198**, 133.
16 R. Prasad, E. Murguly, N. R. Branda, *Chem. Commun.*, 2003, 488.
17 A. G. Montalban, W. Jarrell, E. Riguet, Q. J. McCubbin, M. E. Anderson, A. J. P. White, D. J. Williams, A. G. M. Barrett and B. M. Hoffman, *J. Org. Chem.*,2000, **65**, 2472.
18 H. Nie, A. G. M. Barrett and B. M. Hoffman, *J. Org. Chem.*, 1999, **64**, 6791.
19 N. Kobayashi and T. Fukuda, *J. Am. Chem. Soc.*, 2002, **124**, 8021.
20 P. Y. Reddy, L. Giribabu, C. Lyness, H. J. Snaith, C. Vijaykumar, M. Chandrasekharam, M. Lakshmikantam, J. H. Yum, K. Kalyanasundaram, M. Grätzel and M. K. Nazeeruddin. *Angew. Chem. Int. Ed.*, 2007, **46**, 373.
21 L. J. Yu, X. L. Zhou, Y. H. Yin, Y. W. Liu, R. J. Li and T. Y. Peng, *ChemPlusChem*, 2012, **77**, 1022.
22 E. R. Trivedi, S. Lee, H. Zong, C. M. Blumenfeld, A. G. M. Barrett and B. M. Hoffman, *J. Org. Chem.*, 2010, **75**, 1799.
23 K. Ishii, H. Itoya, H. Miwa, M. Fujitsuka, O. Ito and N. Kobayashi, *J. Phys. Chem. A*, 2005, **109**, 5781.
24 D. Pop, B. Winter, W. Freyer, W. Widdra and I. V. Hertel, *J. Phys. Chem. B*, 2005, **109**, 7826.
25 M. K. Nazeeruddin, R. Splivallo, P. Liska, P. Comte and M. Grätzel, *Chem. Commun.*, 2003, 1456.
26 A. Hagfeldt, G. Boschloo, L. Sun, L. Kloo and H. Pettersson, *Chem. Rev.*, 2010, **110**, 6595.
27 a) L. Girlbabu, V. K. Singh, M. Srinivasu, C. V. Kumar, V. G. Reddy, Y. Soujnya and P. Y. Reddy, *J. Chem. Sci.*, 2011, **123**, 371; b) A. Hagfeldt and M. Grätzel. *Chem. Rev.*, 1995, **95**, 49.
28 J. Jiang, M. Bao, L. Rintoul and D. P. Arnold, *Coord. Chem. Rev.*, 2006, **250**, 424.
29 K. Pei, Y. Wu, A. Islam, Q. Zhang, L. Han, H. Tian and W. Zhu, *ACS Appl. Mater. Inter.*, 2013, **5**, 4986.

30 D. W. De Leeuw, M. M. J. Simenon, A. R. Brown and R. E. F. *Synth. Met.*, 1997, **87**, 53.
31 J. Mack and N. Kobayashi, *Chem. Rev.*, 2011, **111**, 281.
32 H. Miwa, K. Ishii and N. Kobayashi, *Chem. Eur. J.*, 2004, **10**, 4422.
33 B. Lim, G. Y. Margulis, J. H. Yum, E. L. Unger, B. E. Hardin, M. Grätzel, M. D. McGehee and A. Sellinger, *Org. Lett.*, 2013, **15**, 784.
34 R. Kern, R. Sastrawan, J. Ferber, R. Stangl and J. Luther, *Electrochim. Acta*, 2002, **47**, 4213.
35 T. Y. Peng, K. Fan, D. Zhao and J. N. Chen, *J. Phys. Chem. C*, 2010, **114**, 22346.
36 M. Adachi, M. Sakamoto, J. Jiu, Y. K. Ogata and S.J. Isoda, *J. Phys. Chem. B*, 2006, **110**, 13872.
37 A. Zaban, M. Greenshtein and J. Bisquert, *Chem. Phys. Chem.*, 2003, **4**, 859.